Channel and Radar Parameter Estimation with Fractional Delay-Doppler Using OTFS

Sai Pradeep Muppaneni, Sandesh Rao Mattu, and A. Chockalingam

***Abstract*—Orthogonal time frequency space (OTFS) waveform is suited for both communication as well as radar sensing. In this paper, we propose an algorithm for efficient channel estimation at the receiver and range/velocity estimation at the transmitter using OTFS. The algorithm processes received pilot frames for channel estimation at the receiver and data frames echoed from the target/user for range and velocity estimation at the transmitter. A key component in the proposed algorithm is the cancellation of inter-path interference (IPI) in the DD domain. The algorithm works for fractional delay-Doppler which is a source of IPI. The proposed algorithm outperforms other channel estimation schemes and also achieves good root mean square error performance of range and velocity estimation.**

***Index Terms*—OTFS, fractional delay-Doppler, inter-path interference, channel estimation, radar parameter estimation.**

I. Introduction

Orthogonal time frequency space (OTFS) waveform has recently garnered much attention because of its suitability for both communication as well as radar sensing applications [1]-[6]. OTFS waveform is defined and processed in the delay-Doppler (DD) domain. In communications, accurate channel estimation is needed at the receiver for reliable data detection/decoding. In radar sensing, accurate estimation of range and velocity parameters is needed at the transmitter to identify and track targets/users in the sensing environment. This paper is focused on the above two tasks using OTFS, viz., i) channel estimation at the receiver and ii) range and velocity estimation of targets/users at the transmitter by observing the received echoes from them. Specifically, we propose a novel algorithm for efficient estimation of channel at the receiver as well as range/velocity estimation at the transmitter using OTFS. At the receiver, the algorithm operates on the received pilot frame for channel estimation. At the transmitter, the same algorithm operates on the data frames echoed from the target for range and velocity estimation. The proposed algorithm differs from the existing approaches by way of employing a scheme for canceling the DD domain inter-path interference (IPI) arising due to fractional delay-Dopplers. We term the proposed algorithm *DD inter-path interference cancellation* (DDIPIC) algorithm. IPI cancellation in time domain in the context of code division multiple access has been considered in [7]. Here, we perform IPI cancellation in the DD domain.

Several techniques have been proposed in the OTFS literature for channel estimation in the DD domain [8]-[12]. In [8], channel estimation is carried out using an exclusive pilot frame, assuming integer delay-Doppler values. In [9], an embedded pilot frame is considered where both data and pilot symbols are multiplexed in the same frame, with guard symbols in between. Although fractional Doppler values are considered, delays are assumed to take integer values. In [10], sparse Bayesian learning (SBL) algorithm is used to estimate channel coefficients, assuming integer delay and fractional Doppler values. In [11] and [12], SBL algorithm and a modified maximum likelihood estimate (M-MLE) algorithm, respectively, are used to estimate the channel with fractional delays and Dopplers. The M-MLE scheme is shown to perform better than the SBL scheme. A two-step estimation (TSE) algorithm is also proposed in [12]. While the M-MLE algorithm estimates both delay and Doppler jointly, the TSE algorithm individually estimates the delay and Doppler in two steps (estimate the delay in the first step and Doppler in the second step). Our proposed DDIPIC algorithm also estimates the delay and Doppler jointly. A key difference, however, is that we perform refinement of the estimated channel parameters, whereas the M-MLE and TSE algorithms do not, and hence the proposed algorithm achieves better performance.

The use of OTFS waveform for range and velocity estimation in radar sensing applications has been studied in [3]-[6]. The works in [3],[4],[5] on OTFS for communication and sensing consider integer delay-Dopplers. Whereas, the performance of parameter estimation in these schemes are compromised when fractional delay-Dopplers are encountered (which is typical in practical channels). In [6], an iterative scheme for range and velocity estimation with fractional delay-Doppler is proposed. But this scheme assumes perfect knowledge of the number of DD domain paths in the channel. It also considers symbol detection at the receiver/target for which perfect channel knowledge is assumed. In contrast, our DDIPIC algorithm does not assume knowledge of number of DD paths at the transmitter and perfect channel knowledge at the receiver, and it achieves range and velocity estimation performance which is very close to Cramer-Rao lower bound.

II. System model

In OTFS, MN information symbols are multiplexed in the DD domain to obtain the symbol matrix $\mathbf{X}_{\mathrm{DD}} \in \mathbb{A}^{M\times N}$ that is to be transmitted, where $\mathbb{A}$ is the modulation alphabet from where the information symbols are drawn. M and N symbols are placed along the delay and Doppler axes, respectively, with widths T/M and $\Delta f/N$, where $\Delta f = 1/T$. The symbols in the DD domain are converted to frequency-time (FT) domain using inverse symplectic finite Fourier transform (ISFFT), to obtain $\mathbf{X}_{\mathrm{FT}} \in \mathbb{C}^{M\times N}$, as $\mathbf{X}_{\mathrm{FT}} = \mathbf{F}_M\mathbf{X}_{\mathrm{DD}}\mathbf{F}_N^H$, where $\mathbf{F}_M$ is the unitary discrete Fourier transform (DFT) matrix of size M. $\mathbf{X}_{\mathrm{FT}}$ is then converted into a continuous time domain signal using the Heisenberg transform given by $x(t) = \sum_{m=0}^{M-1}\sum_{n=0}^{N-1}\mathbf{X}_{\mathrm{FT}}[m,n]g_{\mathrm{tx}}(t-nT)e^{j2\pi m\Delta f(t-nT)}$, where $g_{\mathrm{tx}}(t)$ is the transmit pulse. The time domain signal $x(t)$ is passed through the channel, which is considered to have P paths in the DD domain, where the pth path has delay τ_p with

The authors are with the Department of ECE, Indian Institute of Science, Bangalore, Karnataka, India, 560012. E-mail: {saimuppaneni; sandeshmattu; achockal}@iisc.ac.in.

$0 < \tau_p < T$ and Doppler shift ν_p. The channel is represented in the DD domain as $h(\tau,\nu) = \sum_{p=1}^{P} \alpha_p \delta(\tau - \tau_p)\delta(\nu - \nu_p)$, where τ_ps and ν_ps are assumed to take fractional values. This can be written in the time domain as $h(t) = \sum_{p=1}^{P} \alpha_p \delta(t - \tau_p) e^{j2\pi\nu_p(t-\nu_p)}$. The received signal thus becomes $y(t) = \sum_{p=1}^{P} \alpha_p x(t - \tau_p) e^{j2\pi\nu_p(t-\nu_p)} + w(t)$, where $w(t)$ is the additive white Gaussian noise (AWGN). The received signal is converted back to DD domain by first converting to the FT domain, using the Wigner transform to obtain $\mathbf{Y}_{\mathrm{FT}} \in \mathbb{C}^{M\times N}$, as $\mathbf{Y}_{\mathrm{FT}}[m', n'] = \int_t y(t) g_{\mathrm{rx}}(t - n'T) e^{-j2\pi m'\Delta f(t-n'T)} dt$, where $m' = 0, 1, \cdots, M-1$, $n' = 0, 1, \cdots, N-1$, and $g_{\mathrm{rx}}(t)$ is the receive pulse. This FT domain signal is converted to DD domain using the symplectic finite Fourier transform (SFFT), to obtain $\mathbf{Y}_{\mathrm{DD}} \in \mathbb{C}^{M\times N}$ as $\mathbf{Y}_{\mathrm{DD}} = \mathbf{F}_M^H \mathbf{Y}_{\mathrm{FT}} \mathbf{F}_N$. $g_{\mathrm{tx}}(t)$ and $g_{\mathrm{rx}}(t)$ are assumed to be rectangular pulses of duration T and amplitude $1/\sqrt{T}$. Using the above equations, the input output relation between $\mathbf{Y}_{\mathrm{DD}}$ and $\mathbf{X}_{\mathrm{DD}}$ can be written as [12]

$$\mathbf{y}_{\mathrm{DD}} = \sum_{p=1}^{P} \alpha_p \mathbf{A}_p(\tau_p, \nu_p)\mathbf{x}_{\mathrm{DD}} + \mathbf{w}, \tag{1}$$

where $\mathbf{w} \in \mathbb{C}^{MN\times 1}$ with entries distributed as i.i.d. $\mathcal{CN}(0,\sigma^2)$, $\mathbf{y}_{\mathrm{DD}} \in \mathbb{C}^{MN\times 1}$, $\mathbf{x}_{\mathrm{DD}} \in \mathbb{A}^{MN\times 1}$ are vectorized forms of $\mathbf{Y}_{\mathrm{DD}}$ and $\mathbf{X}_{\mathrm{DD}}$, respectively, i.e., $\mathbf{y}_{\mathrm{DD}}[q'] = \mathbf{y}_{\mathrm{DD}}[k'M + l'] = \mathbf{Y}_{\mathrm{DD}}[l', k']$, $\mathbf{x}_{\mathrm{DD}}[q] = \mathbf{x}_{\mathrm{DD}}[kM + l] = \mathbf{X}_{\mathrm{DD}}[l, k]$, $l', l = 0, 1, \cdots M-1$, $k', k = 0, 1, \cdots, N-1$, and $q', q = 0, 1, \cdots, MN-1$, and $\mathbf{A}_p$ is an $MN \times MN$ matrix whose entries are given by $\mathbf{A}_p[q', q] = e^{-j2\pi\tau_p\nu_p} a a'$, where $a = \frac{1}{N}\sum_{n=0}^{N-1} e^{-j2\pi n\left(\frac{k'-k}{N} - \frac{\nu_p}{\Delta f}\right)}$, $a' = \frac{1}{M}\sum_{m=0}^{M-1} e^{j2\pi\frac{m}{M}\left(l'-l-M\frac{\tau_p}{T}\right)} r_{\tau_p,\nu_p,k,l'}(m)$, and $r_{\tau_p,\nu_p,k,l'}(m)$ is evaluated using (2) given at the bottom of this page.

A. Integrated communication and sensing architecture

Figure 1 shows the block diagram of the considered communication and sensing architecture. At the transmitter, two types of frames are transmitted, i) pilot frame (marked in yellow), and ii) data frame (marked in purple). The pilot frame is used at the receiver to estimate the DD channel parameters using the proposed algorithm. The estimated channel parameters are then used to detect and decode the transmitted data frames. Since the channel remains almost time-invariant in the DD domain, channel once estimated can be used for multiple data frames. This describes the communication chain from the transmitter to the receiver. Next, the symbols reflected from the receiver (referred to as target in the sensing literature) are received back at the transmitter. These frames (also called echoes), marked in blue, along with the knowledge of the corresponding transmitted frames are used to estimate the sensing parameters corresponding to the target, at the transmitter. The same proposed algorithm is used to estimate the sensing parameters at the transmitter. A key challenge for accurately estimating the channel and radar parameters is the inter-path interference (IPI) resulting due to the fractional DD values as explained in the following subsection.

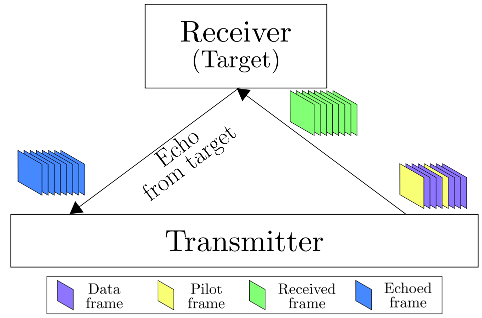

Fig. 1. Communication and sensing architecture.

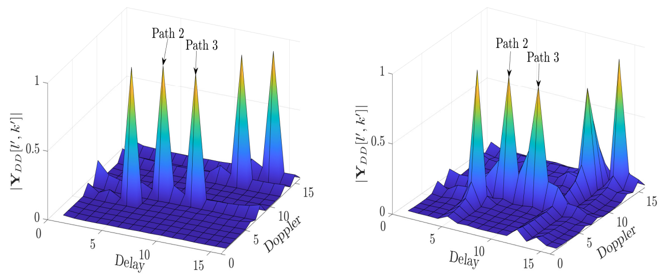

(a) Integer DD (b) Fractional DD

Fig. 2. Received DD domain pilot signal for integer and fractional delay-Dopplers.

B. Inter-path interference

Multiple copies of each transmitted symbol are received when there are P paths ($P > 1$) in the channel. For the pth path, the delay is $\tau_p = \frac{\gamma_p}{M\Delta f}$ and the Doppler is $\nu_p = \frac{\eta_p}{NT}$. In the case of integer DD, the received symbol corresponding to the pth path is localized well in the DD bin specified by the (γ_p, η_p) tuple, where $\gamma_p \in \mathbb{Z}^+$ (the set of all non-negative integers) and $\eta_p \in \mathbb{Z}$ (the set of all integers), as illustrated in Fig. 2a. On the other hand, for the fractional DD case, each transmitted symbol spreads into adjacent bins, resulting in received symbols interfereing with each other (see Fig. 2b). Here, $\gamma_p \in \mathbb{R}^+$ (the set of all non-negative real numbers) and $\eta_p \in \mathbb{R}$ (the set of all real numbers). To obtain Fig. 2a, the fractional DD values used in Fig. 2b are rounded off to the nearest integer. The extent of IPI is dependent on how close or far the channel paths are in the DD grid (e.g., paths 2 and 3 in Fig. 2b exhibit higher IPI compared to other paths). IPI is a source of degradation in the channel/radar parameter estimation performance. To overcome this, we propose an algorithm that cancels the effect of IPI in a sequential manner. This enables the proposed algorithm to perform well for both the channel estimation and radar parameter estimation tasks.

III. Proposed DDIPIC Algorithm

OTFS frames consisting of pilot frames interleaved among the data frames are transmitted at the transmitter (see Fig. 1). For the communication chain, the pilot frames received at the receiver are used to estimate the channel parameters, $(\hat{\alpha}_p, \hat{\tau}_p, \hat{\nu}_p)$ for $p = 1, 2, \cdots, P$, which is then used to

$$r_{\tau_p,\nu_p,k,l'}(m) = \sum_{s=-m}^{M-1-m} e^{j2\pi\frac{sl'}{M}} \left[\left(1 - \frac{\tau_p}{T}\right) e^{j\pi\left(1+\frac{\tau_p}{T}\right)\left(\frac{\nu_p}{\Delta f} - s\right)} \mathrm{sinc}\left(\left(1 - \frac{\tau_p}{T}\right)\left(\frac{\nu_p}{\Delta f} - s\right)\right) + e^{-j2\pi\frac{k}{N}} \left(\frac{\tau_p}{T}\right) e^{\frac{j\pi\tau_p}{T}\left(\frac{\nu_p}{\Delta f} - s\right)} \mathrm{sinc}\left(\left(\frac{\tau_p}{T}\right)\left(\frac{\nu_p}{\Delta f} - s\right)\right)\right]. \tag{2}$$

construct the effective channel matrix, $\hat{\mathbf{H}} = \sum_{p=1}^{P} \hat{\alpha}_p \mathbf{A}_p \in \mathbb{C}^{MN \times MN}$ (see (1)). The estimated channel matrix is used for detection of data symbols in the data frames. For the sensing chain, the reflected OTFS symbols (echoes), along with the knowledge of the transmitted OTFS symbols are used to estimate the range (d) and velocity (v) parameters of the target at the transmitter. Both these tasks are carried out using the proposed DDIPIC algorithm. The algorithm details are as follows. We can write (1) in an alternate form as

$$\mathbf{y} = \sum_{p=1}^{P} \mathbf{b}_p(\tau_p, \nu_p)\alpha_p + \mathbf{w} = \mathbf{B}(\boldsymbol{\tau}, \boldsymbol{\nu})\boldsymbol{\alpha} + \mathbf{w}, \quad (3)$$

where $\mathbf{b}_p(\tau_p, \nu_p) = \mathbf{A}_p \mathbf{x}_{\text{DD}} \in \mathbb{C}^{MN \times 1}$, $\mathbf{B}(\boldsymbol{\tau}, \boldsymbol{\nu}) = [\mathbf{b}_1(\tau_1, \nu_1) \cdots \mathbf{b}_P(\tau_P, \nu_P)] \in \mathbb{C}^{MN \times P}$, $\boldsymbol{\alpha} = [\alpha_1 \cdots \alpha_P]^T \in \mathbb{C}^{P \times 1}$, and $\mathbf{w} \sim \mathcal{CN}(0, \sigma^2) \in \mathbb{C}^{MN \times 1}$. Maximum likelihood (ML) estimate of the $(\boldsymbol{\alpha}, \boldsymbol{\tau}, \boldsymbol{\nu})$-tuple can be evaluated as

$$(\hat{\boldsymbol{\alpha}}, \hat{\boldsymbol{\tau}}, \hat{\boldsymbol{\nu}}) = \underset{\boldsymbol{\alpha}, \boldsymbol{\tau}, \boldsymbol{\nu}}{\text{argmin}} \|\mathbf{y} - \mathbf{B}(\boldsymbol{\tau}, \boldsymbol{\nu})\boldsymbol{\alpha}\|^2, \quad (4)$$

which is an optimization problem with three unknowns. In order to reduce the complexity, we first estimate $\boldsymbol{\tau}$ and $\boldsymbol{\nu}$ and subsequently estimate $\boldsymbol{\alpha}$. Towards this, we note that for a given $(\boldsymbol{\tau}, \boldsymbol{\nu})$, the ML estimate of $\boldsymbol{\alpha}$ is given by

$$\hat{\boldsymbol{\alpha}} = \left[\mathbf{B}^H(\boldsymbol{\tau}, \boldsymbol{\nu})\mathbf{B}(\boldsymbol{\tau}, \boldsymbol{\nu})\right]^{-1} \mathbf{B}^H(\boldsymbol{\tau}, \boldsymbol{\nu})\mathbf{y}. \quad (5)$$

Representing (4) as $(\mathbf{y} - \mathbf{B}(\boldsymbol{\tau}, \boldsymbol{\nu})\boldsymbol{\alpha})^H (\mathbf{y} - \mathbf{B}(\boldsymbol{\tau}, \boldsymbol{\nu})\boldsymbol{\alpha})$, simplifying, and substituting for $\boldsymbol{\alpha}$ from (5) yields the estimate as

$$[\hat{\boldsymbol{\tau}}, \hat{\boldsymbol{\nu}}] = \underset{\boldsymbol{\tau}, \boldsymbol{\nu}}{\text{argmax}} \big[\boldsymbol{\Phi}(\mathbf{B})\big], \quad (6)$$

where $\boldsymbol{\Phi}(\mathbf{B}) = \mathbf{y}^H \mathbf{B}(\boldsymbol{\tau}, \boldsymbol{\nu})(\mathbf{B}^H(\boldsymbol{\tau}, \boldsymbol{\nu})\mathbf{B}(\boldsymbol{\tau}, \boldsymbol{\nu}))^{-1}\mathbf{B}^H(\boldsymbol{\tau}, \boldsymbol{\nu})\mathbf{y}$. Using the estimates $\hat{\boldsymbol{\tau}}$ and $\hat{\boldsymbol{\nu}}$, the estimate of the channel coefficient is obtained as

$$\hat{\boldsymbol{\alpha}} = \left[\mathbf{B}^H(\hat{\boldsymbol{\tau}}, \hat{\boldsymbol{\nu}})\mathbf{B}(\hat{\boldsymbol{\tau}}, \hat{\boldsymbol{\nu}})\right]^{-1} \mathbf{B}^H(\hat{\boldsymbol{\tau}}, \hat{\boldsymbol{\nu}})\mathbf{y}. \quad (7)$$

To solve (6), we employ the proposed DDIPIC algorithm. Estimation of delay and Doppler values is carried out on a path by path basis. Further, this estimation is carried out in two phases, first, the coarse estimation where the search space is over integer multiples of $\left(\frac{1}{M\Delta f}, \frac{1}{NT}\right)$, and second, the fine estimation where the search space is over fractional values. The algorithm runs for a maximum of $P_{\max}$ iterations. In each iteration, one path is estimated so that a maximum of $P_{\max}$ paths are estimated. $P_{\max}$ is chosen to be more than the number of paths P in the channel. The algorithm begins by initializing $\mathbf{B}(\boldsymbol{\tau}, \boldsymbol{\nu}) = [\mathbf{b}_1(\tau_1, \nu_1)\ \mathbf{b}_2(\tau_2, \nu_2)\ \cdots\ \mathbf{b}_{P_{\max}}(\tau_{P_{\max}}, \nu_{P_{\max}})] = \mathbf{0}_{MN \times P_{\max}}$.

Coarse estimation: This is carried out over the search space defined by $\tau \in \left\{\frac{0}{M\Delta f}, \frac{1}{M\Delta f}, \cdots, \frac{L}{M\Delta f}\right\}$, $\nu \in \left\{-\frac{K}{NT}, \cdots, \frac{0}{NT}, \cdots, \frac{K}{NT}\right\}$, where $L = \lceil \tau_{\max} M\Delta f \rceil$, $K = \lceil \nu_{\max} NT \rceil$, and $\tau_{\max}$, $\nu_{\max}$ are the maximum delay and Doppler, respectively. For estimating the first path, $\mathbf{b}_1(\tau_1, \nu_1)$ is evaluated with (τ_1, ν_1) taking all possible combinations of (τ, ν) in the search space. To obtain the optimal coarse estimate (τ_1', ν_1'), we maximize the cost function $\boldsymbol{\Phi}(\mathbf{B})$ in (6).

Fine estimation: This is carried out in a search space around the optimal coarse value obtained in the previous step. Fine estimation of the parameters is carried out iteratively, where the search space is narrowed down as the iterations progress. The search space along the delay and Doppler axes are divided into $\left(2\left\lfloor\frac{m_\tau}{2}\right\rfloor + 1\right)$ and $\left(2\left\lfloor\frac{n_\nu}{2}\right\rfloor + 1\right)$ equally spaced bins, respectively. This iterative procedure is presented in **Algorithm 1**, where $\Gamma = \left\{0, \cdots, \lfloor\frac{m_\tau}{2}\rfloor\right\}$ for $\tau_1' = 0$ and $\Gamma = \left\{-\lfloor\frac{m_\tau}{2}\rfloor, \cdots, 0, \cdots, \lfloor\frac{m_\tau}{2}\rfloor\right\}$ for $\tau_1' > 0$, $\Lambda = \left\{-\lfloor\frac{n_\nu}{2}\rfloor, \cdots, 0, \cdots, \lfloor\frac{n_\nu}{2}\rfloor\right\}$, and the operator $\otimes$ denotes the Cartesian product of two sets. At the end of **Algorithm 1**, fine estimates for the first path $\hat{\tau}_1$ and $\hat{\nu}_1$ are obtained.

Algorithm 1 Fine estimation of channel parameters

- **Inputs:** Coarse estimates (τ_p', ν_p'), refinements (m_τ, n_ν), convergence indicators $(\epsilon_\tau, \epsilon_\nu)$, and max_iter
- **Initialize:** $s = 1$, $\hat{\tau}^{(1)} = \tau_p'$, and $\hat{\nu}^{(1)} = \nu_p'$
- **repeat**
  - search width in delay, $w_\tau^{(s)} = \frac{1}{M\Delta f m_\tau^{s-1}}$
  - search width in Doppler, $w_\nu^{(s)} = \frac{1}{NT n_\nu^{s-1}}$
  - $\mathbf{F}^{(s)} = \left\{w_\tau^{(s)}\Gamma + \hat{\tau}^{(s)}\right\} \otimes \left\{w_\nu^{(s)}\Lambda + \hat{\nu}^{(s)}\right\}$, search space for fractional DD
  - $\hat{\tau}^{(s+1)}, \hat{\nu}^{(s+1)} = \underset{(\tau,\nu)\in\mathbf{F}^{(s)}}{\text{argmax}}\ \Phi(\mathbf{B})$
- **update** $s = s + 1$
- **until** s = max_iter or $\left(|\hat{\tau}^{(s+1)} - \hat{\tau}^{(s)}| < \epsilon_\tau \text{ and } |\hat{\nu}^{(s+1)} - \hat{\nu}^{(s)}| < \epsilon_\nu\right)$
- **Output:** $\hat{\tau}_p = \hat{\tau}^{(s+1)}$ and $\hat{\nu}_p = \hat{\nu}^{(s+1)}$

For the estimation of parameters of the tth path ($t > 1$), columns $1, 2, \cdots, t-1$ in $\mathbf{B}$ are filled using the already obtained $(\hat{\tau}_p, \hat{\nu}_p)$s, $p = 1, 2, \cdots, t-1$. The coarse estimates for τ_t and ν_t are obtained by maximizing the cost function in (6) over different values of (τ, ν) in the tth column of $\mathbf{B}$, as described in the coarse estimation stage. This is followed by the fine estimation stage using **Algorithm 1**, which gives the fine estimates $(\hat{\tau}_t, \hat{\nu}_t)$.

Stopping criterion: At the end of fine estimation for tth path, $t > 1$, the matrix $\mathbf{B}(\hat{\boldsymbol{\tau}}, \hat{\boldsymbol{\nu}})$ is obtained, using which $\hat{\boldsymbol{\alpha}}$ is obtained using (7). A residue vector $\mathcal{E}^{(t)}$ is obtained as $\mathcal{E}^{(t)} = \mathbf{y} - \mathbf{B}(\hat{\boldsymbol{\tau}}, \hat{\boldsymbol{\nu}})\hat{\boldsymbol{\alpha}}$. If $\|\mathcal{E}^{(t)} - \mathcal{E}^{(t-1)}\|^2 > \epsilon$ and $t < P_{\max}$, then the algorithm makes $t = t + 1$ and continues with the estimation of the next path. The algorithm stops if $\|\mathcal{E}^{(t)} - \mathcal{E}^{(t-1)}\|^2 < \epsilon$ or $t = P_{\max}$.

Refinement of parameter estimates: After the estimation of tth path, $1 < t < P_{\max}$, if the stopping criterion is not met, we refine the previously obtained estimates before estimating the parameters of the $(t+1)$th path. This refinement proceeds as follows. For the zth path, with $1 \leq z \leq t$, we use the estimates $(\hat{\tau}_i, \hat{\nu}_i)$s with $i = 1, 2, \cdots, z-1, z+1, \cdots, t$, to obtain the matrix $\mathbf{B}$ (i.e., fill all the columns in $\mathbf{B}$ except the zth column). We then evaluate the refined estimates of the zth path again, by optimizing the cost function in (6) for the zth column of $\mathbf{B}$. This is carried out first over the coarse search space and then over the fine search space. Following this, the estimate of parameters of the $(t+1)$th path is obtained using the refined estimates of all the paths till t. This is illustrated with the following example. When $t = 3$, three paths are estimated, and the stopping criterion is not met, then

- 1st path is refined using the 2nd and 3rd paths (both unrefined),
- 2nd path is refined using the refined first path and the 3rd path (unrefined), and
- 3rd path is refined using the refined 1st and 2nd paths.

The estimate of the parameters of the 4th path is obtained

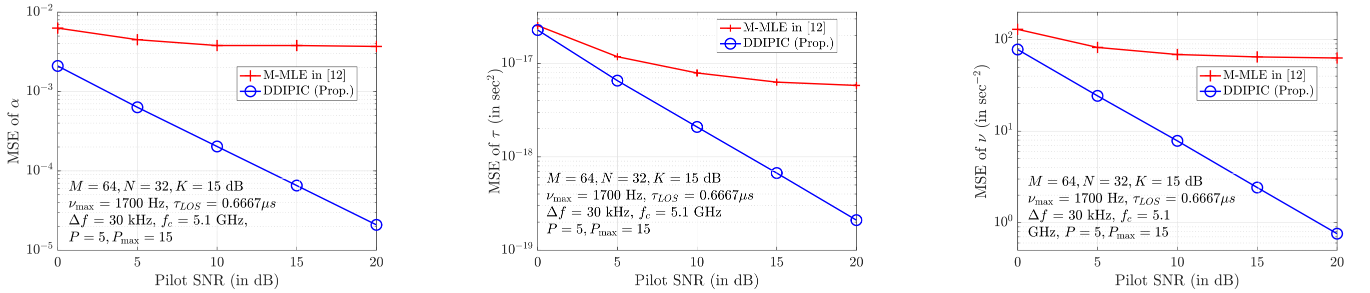

(a) Channel coefficients (b) Delay (c) Doppler

Fig. 3. MSE of estimated parameters as a function of pilot SNR.

TABLE I
COMPUTATIONAL COMPLEXITY FOR COST FUNCTION.

Operation	Complex multiplications	Complex additions	Total complexity
$\boldsymbol{\Xi} = \mathbf{y}^H \mathbf{B}(\boldsymbol{\tau}, \boldsymbol{\nu})$	$P_{\max}MN$	$P_{\max}(MN-1)$	$2P_{\max}MN - P_{\max}$
$\boldsymbol{\Upsilon} = \mathbf{B}^H(\boldsymbol{\tau}, \boldsymbol{\nu})\mathbf{B}(\boldsymbol{\tau}, \boldsymbol{\nu})$	$P_{\max}^2 MN$	$P_{\max}^2(MN-1)$	$2P_{\max}^2 MN - P_{\max}^2$
$\boldsymbol{\Upsilon}^{-1}$	-	-	$\mathcal{O}(P_{\max}^3)$
$\boldsymbol{\Xi}\boldsymbol{\Upsilon}^{-1}$	$P_{\max}^2$	$P_{\max}(P_{\max}$-1)	$2P_{\max}^2$- $P_{\max}$
$\boldsymbol{\Xi}\boldsymbol{\Upsilon}^{-1}\boldsymbol{\Xi}^H$	$P_{\max}$	$P_{\max}$-1	$2P_{\max}$-1

TABLE II
COMPLEXITY IN DIFFERENT STAGES OF ESTIMATION.

Estimation stage	**Complexity** (value × C)
Coarse estimation	$C' = (L+1)(2K+1)P_{\max}$
Fine estimation	$C'' = \left(2\lfloor\frac{m_\tau}{2}\rfloor+1\right)\left(2\lfloor\frac{n_\nu}{2}\rfloor+1\right)P_{\max}$
Refinement	$\left(\frac{(P_{\max}-1)P_{\max}}{2}-1\right)(C'+C'')$
Channel coefficient	1

using the refined 1st, 2nd, and 3rd path estimates. We note that an estimated path maybe refined multiple times depending on how many paths are estimated before convergence of the DDIPIC algorithm. For example, when $P_{\max} = 3$, after the estimation of two paths, both first and second paths are refined. Next, after the third path is estimated, first, second, and third paths are refined. So, at the end of the DDIPIC algorithm, first and second paths are refined twice and third path is refined once. This multiple refinements possibility allows effective cancellation of interference between different paths.

Remark on choice of ϵ: We note that the algorithm defined above can have multi-checks and misses depending on the value chosen for ϵ. A high value of ϵ can lead to paths (with small amplitudes) being missed, while a small value of ϵ can lead to false paths or multi-checks, wherein an already estimated path is picked for estimation again. Simulations have shown that the chances of multi-checks and misses are reduced when ϵ is chosen to be about 1% of the noise energy in the frame. Consequently, we have used ϵ to be $0.01MN\sigma^2$.

Complexity: Table I shows the computation complexity of the proposed estimator (6) in terms of number of complex additions and multiplications. The sum of the last column, $C = 2P_{\max}MN + 2P_{\max}^2 MN + P_{\max}^2 + \mathcal{O}(P_{\max}^3) - 1$ is the total number of operations required to compute (6). Table II shows the maximum number of times the cost function in (6) is evaluated in each stage of estimation. The sum of the last column multiplied with C denotes the maximum complexity of the proposed algorithm.

IV. RESULTS AND DISCUSSIONS

In this section, we present the numerical results on the performance of the proposed DDIPIC algorithm. We consider $M = 64$, $N = 32$, $\Delta f = 30$ kHz, and $f_c = 5.1$ GHz. The channel is assumed to have $P = 5$ resolved paths with a line of sight (LOS) path and a Rice factor of 15 dB [12]. The delay of the first and second paths are taken to be $0.667\mu s$, $0.867\mu s$, respectively, and the delays of other paths are uniformly distributed in $(0.867\mu s, 7\mu s]$. Doppler frequencies for all the paths are generated from Jake's Doppler spectrum using $\nu_p = \nu_{\max}\cos(\theta_p)$ where θ_p is uniformly distributed in $(0, 2\pi]$ and $\nu_{\max}$ is 1700 Hz. The fixed absolute squared value of the channel gain of LOS path is taken according to the Rice factor, and exponential power delay profile is used for the other paths as in [12]. Further, $m_\tau = n_\nu = 10$, $\epsilon_\tau = 10^{-10}$, $\epsilon_\nu = 10^{-2}$, $P_{\max} = 15$ and $\epsilon = 0.01MN\sigma^2$.

A. Channel estimation performance at receiver

1) MSE performance of channel parameters: Figure 3 shows the MSE performance of the channel parameters obtained using the proposed DDIPIC algorithm for the LOS path. Specifically, MSE of the channel coefficient, delay, and Doppler values are presented in Figs. 3a, 3b, and 3c, respectively. The MSE performance of the channel parameters obtained using the M-MLE algorithm is also presented for comparison. It is seen that for all the channel parameters, the MSE performance using the proposed DDIPIC is observed to decrease almost linearly with pilot SNR. On the other hand, the MSE performance of M-MLE algorithm is seen to floor.

2) NMSE performance: Normalized mean square error (NMSE) is evaluated as $\mathbb{E}\left[\frac{\|\mathbf{H}-\hat{\mathbf{H}}\|_F^2}{\|\mathbf{H}\|_F^2}\right]$. Figure 4 shows the NMSE performance of the channel matrix obtained using the proposed DDIPIC algorithm. The NMSE performance obtained using the M-MLE algorithm in [12] is also presented for comparison. It is seen that the NMSE performance of both the schemes decrease almost linearly with pilot SNR. However, the NMSE performance with the proposed DDIPIC is better when compared to that of the M-MLE scheme. For example, NMSE value of -30 dB is obtained at around 10 dB of pilot SNR with the proposed scheme, as opposed to 15 dB with the M-MLE scheme.

3) BER performance: Figure 5 shows the BER versus SNR performance of the proposed DDIPIC algorithm for a pilot SNR of 10 dB. BER performance with perfect CSI is also added for reference along with the performance of M-MLE scheme. Minimum mean square error (MMSE) detection is used and the data symbols are drawn from 64-QAM modulation alphabet. First, it is observed that the proposed DDIPIC algorithm achieves better performance compared to the M-MLE scheme. For example, a BER of 10^{-3} is achieved at 24 dB for the proposed scheme, while it is achieved at about

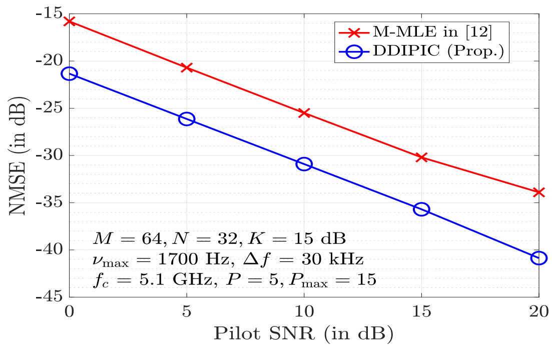

Fig. 4. NMSE performance of the proposed DDIPIC algorithm as a function of pilot SNR.

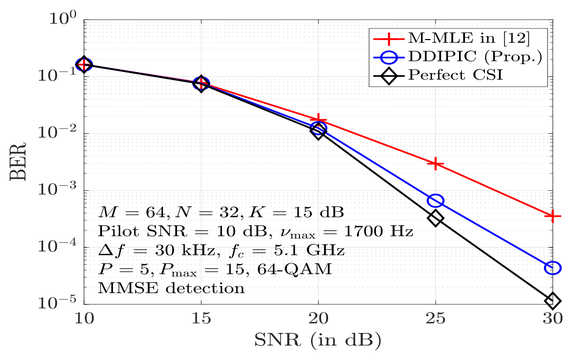

Fig. 5. BER performance of the proposed DDIPIC algorithm as a function of SNR.

28 dB for the M-MLE scheme. This performance gain is attributed to the refinement of parameter estimates achieved through IPI cancellation in the proposed algorithm. Further, the proposed algorithm is observed to perform close to that with perfect CSI. Figure 6 shows the BER performance of the proposed DDIPIC algorithm as a function of $P_{\max}$ at 10 dB pilot SNR and 20 dB data SNR. Performance with perfect CSI at 20 dB data SNR is also plotted for comparison. It is seen that as the number of iterations increase, the BER converges close to the performance with perfect CSI. This is because, due to IPI cancellation, the channel estimates get more refined as the number of iterations is increased. Even two or three iterations show significant improvement in BER.

B. Radar parameter estimation performance at transmitter

In this subsection, we present range and velocity estimation performance of the proposed algorithm with $M = 64$, $N = 50$, $f_c = 5.89$ GHz, and $\Delta f = 156.25$ kHz. The range and velocity of the target are considered to be 20 m and 80

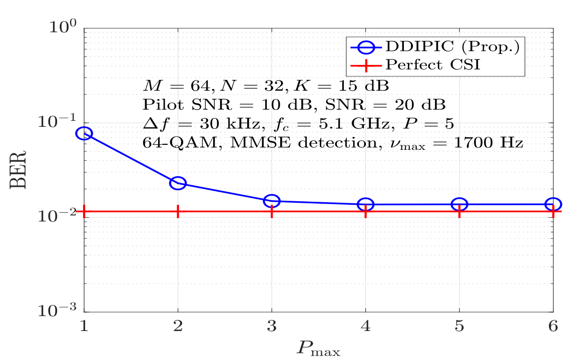

Fig. 6. BER performance of the proposed DDIPIC algorithm as a function of $P_{\max}$.

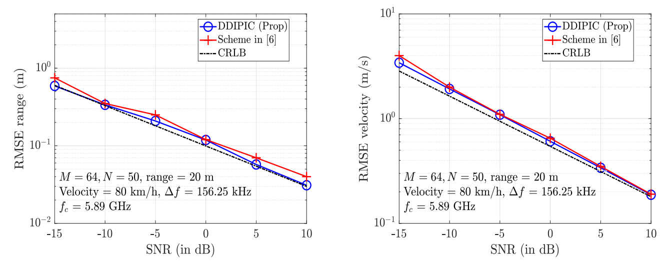

(a) RMSE of range (b) RMSE of velocity

Fig. 7. RMSE of range and velocity as a function of SNR.

km/h, respectively, The above parameters are as in [6]. Figure 7a shows the root mean square error (RMSE) performance of range estimation as a function of SNR achieved with the proposed DDIPIC algorithm. The performance achieved with the scheme in [6] is also shown for comparison. Further, the Cramer-Rao lower bound (CRLB) for the considered system is also plotted. It is seen that the proposed scheme and the scheme in [6] perform similarly and this performance is close to the CRLB. Figure 7b shows the RMSE performance of velocity estimation as a function of SNR for the proposed algorithm and the scheme in [6] along with the CRLB. Similar to the delay estimation performance, both the approaches exhibit similar velocity estimation performance that is close to CRLB. However, we note that the scheme in [6] assumes the knowledge of the number of paths, whereas the proposed DDIPIC algorithm requires no such knowledge.

References

[1] R. Hadani et al., “Orthogonal time frequency space modulation,” *Proc. IEEE WCNC’2017*, pp. 1-6, Mar. 2017.

[2] Z. Wei et al., “Orthogonal time-frequency space modulation: a promising next-generation waveform,” *IEEE Wireless Commun. Mag.*, vol. 28, no. 4, pp. 136-144, Aug. 2021.

[3] W. Yuan, Z. Wei, S. Li, J. Yuan, and D. W. K. Ng, “Integrated sensing and communication-assisted orthogonal time frequency space transmission for vehicular networks,” *IEEE J. Sel. Topics in Signal Process.*, vol. 15, no. 6, pp. 1515-1528, Dec. 2021.

[4] P. Raviteja, K. T. Phan, Y. Hong, and E. Viterbo, “Orthogonal time frequency space (OTFS) modulation based radar system,” *Proc. IEEE Radar Conf.*, pp. 1-6, Apr. 2019.

[5] S. Li, W. Yuan, C. Liu, Z. Wei, J. Yuan, B. Bai, and D. W. K. Ng, “A novel ISAC transmission framework based on spatially-spread orthogonal time frequency space modulation,” *IEEE J. Sel. Areas Commun.*, vol. 40, no. 6, pp. 1854-1872, Jun. 2022.

[6] L. Gaudio, M. Kobayashi, G. Caire, and G. Colavolpe, “On the effectiveness of OTFS for joint radar parameter estimation and communication,” *IEEE Trans. Wireless Commun.*, vol. 19, no. 9, pp. 5951-5965, Sep. 2020.

[7] K. Hooli, M. Juntti, and M. Latva-Aho, “Inter-path interference suppression in WCDMA systems with low spreading factors,” *Proc. IEEE VTC’1999*, vol.1, pp. 421-425, Sep. 1999.

[8] M. K. Ramachandran and A. Chockalingam, “MIMO-OTFS in high-Doppler fading channels: signal detection and channel estimation,” *Proc. IEEE GLOBECOM’2018*, pp. 206–212, Dec. 2018.

[9] P. Raviteja, K. T. Phan, Y. Hong, and E. Viterbo, “Embedded pilot-aided channel estimation for OTFS in delay-Doppler channels,” *IEEE Trans. Veh. Tech.*, vol. 68, no. 5, pp. 4906-4917, May 2019.

[10] F. Liu, Z. Yuan, Q. Guo, Z. Wang, and P. Sun, “Message passing based structured sparse signal recovery for estimation of OTFS channels with fractional Doppler shifts,” *IEEE Trans. Wireless Commun.*, vol. 20, no. 12, pp. 7773-7785, Dec. 2021.

[11] Z. Wei, W. Yuan, S. Li, J. Yuan, D. W. K. Ng, “Off-grid channel estimation with sparse Bayesian learning for OTFS systems,” *IEEE Trans. Wireless Commun.*, vol. 21, no. 9, pp. 7407-7426, Sep. 2022.

[12] I. A. Khan and S. K. Mohammed, “Low complexity channel estimation for OTFS modulation with fractional delay and Doppler,” arXiv:2111.06009 [cs.IT], Nov. 2021.